Treatment Planning for Internal Radionuclide Therapy: Three-Dimensional Dosimetry for Nonuniformly Distributed Radionuclides

George Sgouros, Glenn Barest, Jose Thekkumthala, Chen Chui, Radhe Mohan, Rodney E. Bigler, and Pat B. Zanzonico

Department of Radiology, Division of Nuclear Medicine, The New York Hospital-Cornell Medical Center, New York, New York and Department of Medical Physics, Memorial Sloan-Kettering Cancer Center, New York, New York

A calculational approach is described that provides the spatially varying radiation absorbed dose, presented as isodose contours superimposed on CT images, from nonuniform and/or irregular cumulated activity distributions. CT images are read from magnetic tape and are displayed on a high-resolution color graphics display monitor. Source tissue geometries are defined on a series of contiguous CT images automatically (by an edge detection algorithm) or manually (using a trackball), thereby obtaining a three-dimensional representation of the various source volumes of activity. Dose calculations are performed using a radionuclide-specific absorbed dose point kernel in the form of a lookup table. The method described yields the spatially varying dose delivered to tumor and normal tissue volumes from a patient-specific cumulated activity distribution in a clinically implementable manner. This level of accuracy in determining normal tissue and tumor doses may prove valuable in the evaluation and implementation of radionuclides and radiolabeled compounds for therapeutic purposes.

J Nucl Med 1990; 31:1884–1891

Conventional approaches to the determination of absorbed dose in humans from internally deposited radionuclides and labeled compounds generally include the collection of serial blood, total-body, and organ time-activity data. Integration of these data yield source volume cumulated activities. Assuming a uniform distribution of cumulated activities within each source region and a uniform deposition of radiation energy within each target region, the average absorbed dose to a given target region from a given source region is estimated for a specific anatomic model [e.g., Standard Man (*1*)]; the total target volume absorbed dose is then the summation of all of the source volume absorbed dose contributions. This approach was developed by the Medical Internal Radiation Dose (MIRD) Committee of the Society of Nuclear Medicine (*2–4*). Estimation of average absorbed dose has proven to be highly useful for the determination of radiation doses from internally deposited radionuclides, particularly when the radionuclide is used for diagnostic purposes (e.g., where normal tissues doses are well below tissue radiation tolerance). For purposes of radiation therapy, where an accurate estimation of the radiation dose to therapy-limiting tissues is required in order to maximize the therapeutic benefit, clinically implementable methods for assessment of the spatially varying radiation dose over normal and tumor-containing tissue volumes similar to those now used for external beam radiation therapy are needed.

Received Sept. 11, 1989; revision accepted Apr. 19, 1990.

For reprints contact: George Sgouros, Division of Nuclear Medicine, Rm ST-221, The New York Hospital - Cornell Medical Center, 525 East 68th St., New York, NY 10021.

METHODOLOGY

Basic Approach

The method we have developed (*5*) requires the following input: a user-selectable radionuclide-specific point source kernel (stored as a lookup table); a collection of contours, derived from patient CT scans, comprising a three-dimensional matrix that defines one or more source volumes; a corresponding set of independently determined cumulated activity concentrations; and a target plane (generally chosen to intersect a therapy-limiting or target tissue). The algorithm convolves the source volume cumulated activity distribution with the point source kernel to yield a two-dimensional matrix of dose values corresponding to points on the target plane. The dose matrix is converted into a set of color-coded isodose contours which are displayed superimposed on the CT image corresponding to the target plane.

Briefly, the dose calculation proceeds as follows. The distance between a given voxel inside an activity-containing source volume and a point on the target plane is calculated. This distance is then found in the lookup table of dose versus distance (i.e., the point source kernel) to obtain the dose per unit cumulated activity; this dose is multiplied by the cumu-

lated activity in the source voxel and assigned to the given target plane point. The total absorbed dose to the target point is then obtained by summing the contribution from each source voxel. The procedure is repeated for the next target point until a total dose value has been assigned to all points on the two-dimensional grid defining the target plane.

The approach described relies on image-based anatomical information to define activity containing source volumes. The basic algorithm has been incorporated into a VAX/VMS FORTRAN software package, Internal Dosimetry for Treatment Planning (IDTP), consisting of 10 programs, each of which controls a well-defined stage of the treatment planning process. The support structure (i.e., CT tape translation, image display and handling, region of interest definition, etc.) of an external beam three-dimensional treatment planning program, developed at the Medical Physics Department of Memorial Sloan-Kettering Cancer Center (*6*), was maintained for IDTP. Use of this structure (*6–8*) for internal dosimetry maintains compatibility with an established treatment planning environment, thereby facilitating incorporation of continuing improvements in external beam treatment planning software.

The Point Source Dose Kernel

Appropriate selection of a point source kernel for a given dosimetry calculation is critical. The point source kernel is a table of absorbed doses versus the corresponding distances from a point source. The first dose value (corresponding to the first distance entry r_1) is equal to the energy deposited in a sphere of radius r_1 centered at the source point divided by the mass of the sphere. Remaining dose values are equal to the energy deposited within a spherical shell of inner and outer radii r_{i-1} and r_i, respectively, for a distance r_i from the source point divided by the mass of the spherical shell. The point source kernel incorporates the radionuclide [in the form of its emission spectrum (*9*)], the absorbing medium, and the scale and resolution of the calculation (determined by the point kernel's list of distances).

In anticipation of the need to select point kernels appropriate to the emissions and their energies of each radionuclide, differing scales of the dose calculation, and differing compositions of the stopping medium; we have adopted an approach that permits one to insert point kernels into the treatment planning calculation. The point kernel is provided as input in the form of an appropriately formatted file containing a dose-distance table. The point-kernel generation process (e.g., experimental measurements, analytical or Monte Carlo calculations) and the dose calculation process are therefore distinct. A variety of dose point kernels are available. These include the tables of Berger for photons and for monoenergetic electrons (*10–12*), the tables of Cross for beta emitters (*13*), and the analytical dose point kernels of Prestwich et al. for beta emitters (*14*). In addition, analytical dose point kernels for alpha and for monoenergetic electron emitters have been derived (*15*) from the empirical range-energy relations of Polig (*16*) and Cole (*17*), respectively.

Our IDTP-based dosimetry calculations were obtained using a point source kernel generated by the Electron Gamma Shower (EGS) Monte Carlo simulation program (*18*). The EGS code allows one to define the point source emission spectrum as a series of distinct emissions, each characterized by its energy, frequency and type (e.g., photon or electron). A continuous energy beta-decay spectrum should be approximated by partitioning the spectrum into a series of discrete energies and their corresponding frequencies (*19*) when the maximum range exceeds the spatial resolution of the calculation. The chemical composition of the absorbing medium may also be defined; the illustrative calculations presented in this paper are for a water-equivalent medium. Since the point kernel is generated assuming an infinite medium of uniform composition, the IDTP calculations do not take into account tissue inhomogeneities within organs (e.g., tumors) or transition effects (*20*) at the interface between an organ and its surroundings (e.g., bone-soft tissue).

We have chosen EGS-derived point kernels for our calculations because EGS is flexible and well-documented, has been experimentally well characterized, and most importantly is comparable in accuracy to other available point kernels (*21*). The current version of EGS, EGS4, is applicable to electron energies down to 10 keV and photon energies down to a few keV when water is the stopping medium (*22*). It is important to note that given the dimensional scale of the CT-based treatment planning calculation the range of low-energy electron emissions is less than voxel dimensions and their dose contribution is therefore included assuming absorption at the point of emission.

An alternative to EGS4 at low energies is ETRAN, the Monte Carlo code developed by Berger and Seltzer for applications at energies of a few MeV and lower (*23*). The major differences in electron transport between the two codes at lower energies lie in the manner in which residual electron energy is handled once the electron history is terminated and in the bremsstrahlung cross section (*21*). When an electron history is terminated in ETRAN, the remaining electron energy is deposited at a randomly chosen point between zero and the residual range of the electron. In contrast, EGS deposits the residual energy at the point where the history is terminated. The EGS approximation is appropriate for CT-based treatment planning since the scale of the calculation is much larger than the residual range of low-energy electrons. EGS's treatment of bremsstrahlung differs from that of ETRAN in that the bremsstrahlung cross-section is underestimated at lower electron energies while the X-ray yield is overestimated. In most applications (and especially in low atomic number media such as water), however, this is of little consequence since the bremsstrahlung energy for low-energy electrons is a small fraction of the total electron energy. These differences in the handling of low-energy electrons do not result in very significant calculational differences; the EGS results for low-energy electron transport in water do not deviate by more than 5% from the ETRAN results (*21*). For low-energy photons, EGS includes Rayleigh scattering, which is not included in ETRAN.

Source Volume Specification

A source volume is a user-defined volume of arbitrary shape (subject to the constraints of the finite image matrix) which is assigned an independently determined cumulated activity concentration. Patient-specific source volumes are generated from CT images by first identifying the structure or structures to be assigned cumulated activity concentrations and, starting from the first (most superior or most inferior) CT slice in

which the structure is visible, drawing a contour around the periphery of each as seen on each of the contiguous CT slices. Contours may be drawn either manually using a trackball or automatically using an edge detection algorithm. The result is a series of contours (each associated with a particular CT slice) which when stacked form a representation of the three-dimensional surface of the structure of interest (see Figures 1 and 2). The set of contours are grouped and identified by a user-provided "structure name." Each surface thus defined forms the boundary of a source volume. A cumulated activity concentration is then assigned to points within each such volume. In this manner, one may define any number of patient-specific, activity-containing volumes. A nonuniform activity distribution within a particular volume may be approximated by dividing the structure into substructures, each of which is assigned a distinct cumulated activity concentration. This approach for assigning tissue cumulated activities is practical given the relatively coarse spatial resolution and limited contrast of planar and SPECT imaging and the resulting small number of identifiable regions of interest (ROIs) in even large anatomic structures (*24*). The degree to which a set of contours represents the actual structure geometry will depend on the thickness and inter-slice spacing of the CT slices, the radiographic contrast, and the accuracy with which the contours are drawn. Although the contour representation of a particular structure may be better resolved in a CT study with a smaller interslice spacing and slice thickness, additional contour drawing and computational time are required. The CT slice thickness should be made sufficiently small for a reasonable number of CT slices to span the source volume. If the source volumes are spanned by more than ten or less than three CT slices, for example, one should consider increasing or decreasing the CT slice thickness, respectively.

Once the source volumes are defined as sets of contours they may be displayed in a "wire-frame" image. This is shown in Figure 1, which depicts a set of liver and intra-hepatic tumor contours. Such a display provides an overall view of the calculational volume and relationships among the source and target volumes. As shown in Figure 2, a different view or perspective may be displayed by real-time "rotation" of the gantry or the couch using the trackball. One may also exclude one or more contour sets thereby providing an unobscured view of specific structures of interest. For example, the set of contours corresponding to the body surface (depicted in yellow in Figure 1) have been "turned off" in Figure 2.

Target Region Specification

The two-dimensional area on a plane within which isodose contours are to be computed and displayed is the target region. This region is usually defined within a single transverse CT image. One selects a slice containing a critical (i.e., dose-limiting) organ or target structure (e.g., tumor). Superimposed upon this image is a grid whose spacing, size (length and width), and position may be adjusted by the user (Cf. Fig. 3). The grid determines the spacing of points (defined by the intersecting grid lines) at which doses are computed. The grid size and position specify the target region over which isodose contours will be generated. In order to optimize computation time, the grid spacing and size should be commensurate with the detail and overall size, respectively, of the pertinent anatomy. The target region may include regions within and/or outside the cumulated activity-containing source volume.

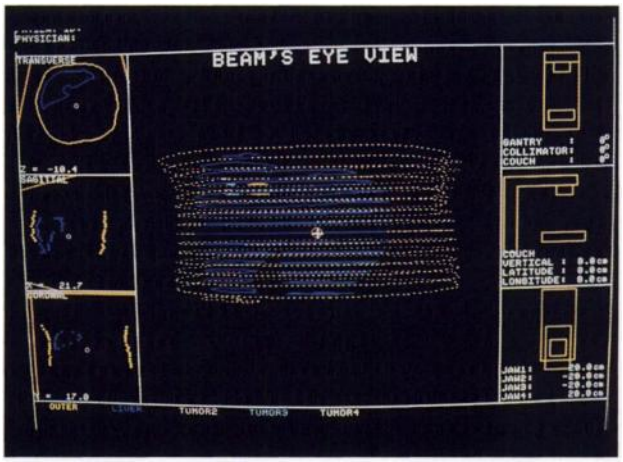

FIGURE 1
An anterior view of a wire frame diagram depicting the periphery of the body in yellow, the liver in dark blue, and three small tumors in pink, light blue, and orange, Each set of contours represents contours drawn from the anatomy of the patient as shown on a consecutive series of CT images. To the left of the wire frame diagram are shown a transverse, sagittal, and coronal slice (each taken through the mid-plane, at the level of the cross-hair, of the respective view). To the right of the wire frame diagram a view of the gantry and couch is depicted from the front, from the side and from above in the top, middle and bottom panel, respectively.

Dose Calculations

Once a point kernel, each source volume and its cumulated activity concentration, and a target plane have been specified, the absorbed dose calculation is performed as follows. The distance between a source point and a target point is calculated. This distance is used to find, by interpolation, the corresponding dose contribution in the point kernel table. This process is repeated until all source points have been exhausted. The dose value assigned to the target point is the

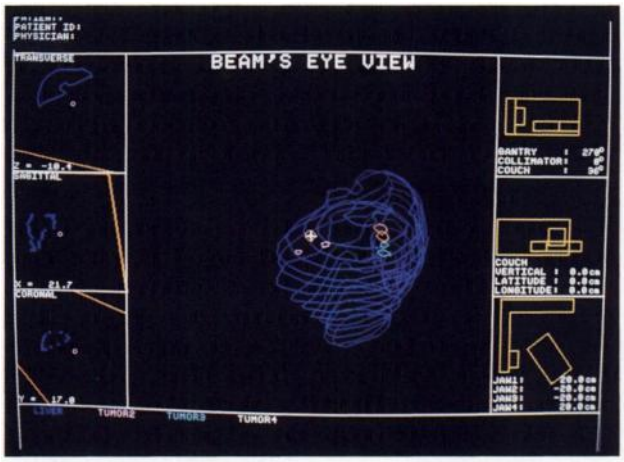

FIGURE 2
An oblique view of the wire frame diagram depicted in Figure 1. The set of contours representing the periphery of the body have been "turned off" to better display the liver and the intrahepatic tumors. To the right of the wire frame diagram the gantry and couch orientations used to obtain this view are depicted.

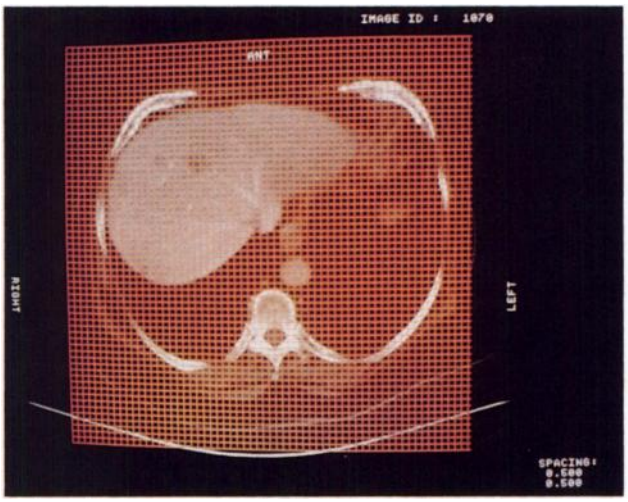

FIGURE 3
The grid used to define the region for which isodose contours will be generated is shown overlaid on a CT image through the liver.

sum of the individual contributions from all of the source points. The algorithm then shifts to another target point and the entire procedure is repeated. Mathematically the dose, D_i, to target point i may be expressed as:

$$D_i = \sum_j K(r_{ij}) \times A_j, \quad (1)$$

where

r_{ij} = distance between source point j (at x_j, y_j, z_j) and target point i (at x_i, y_i, z_i)

$$= \sqrt{(x_i-x_j)^2+(y_i-y_j)^2+(z_i-z_j)^2},$$

$K(r_{ij})$ = point kernel lookup table dose at a distance r_{ij},

A_j = cumulated activity at source point j
$= [A](dl)^3$

where

[A] = the cumulated activity concentration in the source volume

dl = the length of the source voxel edge.

Two important practical problems had to be resolved to implement this algorithm.

1. Given a set of coordinates defining a closed surface within a three-dimensional matrix of points, how does one identify points inside the surface in a computationally efficient manner? This is essential in order to distinguish target points inside the source volume from target points outside the source volume. The technique to determine whether a point lies inside a closed surface is based on determining the number of times a ray emanating from the target point intersects the closed surface of the source (*6, 20*). If the number of intersections is odd, then the point is inside the surface; otherwise, it is outside or on the surface.

2. Will the dose-calculation algorithm hold when calculating the absorbed dose to target points inside the source volume? To answer this, we must first rigorously define both a target and a source point. A source point may be thought of as a point at the center of a small cube of edge dl, volume dl^3, and cumulated activity $[A] \times dl^3$, where [A] is the cumulated activity concentration within the source volume. The target plane points define the coordinates for which dose calculations are to be performed; no volume is associated with these points. Consider a target point inside a source volume. Proceeding according to the algorithm, the distance between the target point and every point in the source volume is calculated and used to obtain a dose value from the point kernel. Each such dose value is multiplied by the source point cumulated activity and is then added to the dose sum for the given target point. Now consider a point kernel for a pure low-energy electron emitter. Let us assume that the electron range is r μm and that the total energy deposited within a sphere of radius r μm from a point source at the center is E_0. Assuming the distance r_1 corresponding to the first entry in the point kernel is greater than r μm and letting V_1 equal the volume of a sphere of radius r_1, the point kernel entries would be as follows: $(r_1, E_0/V_1)$, $(r_2, 0)$, . . ., $(r_N, 0)$. The first entry reflects the energy density (per disintegration) resulting from a point source inside a sphere of radius r_1, while the remaining entries are all zero (reflecting the short range of the emission). Because the target and source points are generally not congruent, the distance between the target point and even the nearest source point may be greater than r_1. The algorithm would yield in this case an erroneous absorbed dose of zero. The solution we have implemented is based upon assigning a mean local dose to target points inside the source volume. The mean local dose is evaluated within a spherical volume defined by the diagonal distance across a source voxel. The steps required to incorporated assignment of the mean local dose into the algorithm are as follows:

1. Calculate the diagonal distance (largest distance) across a source voxel ($= dl \times \sqrt{3}$).
2. The energy deposited in a sphere with diameter equal to the diagonal calculated in Step 1 is obtained in the following manner. The first entry in the point kernel table, E_1/V_1, is multiplied by the volume V_1 of a sphere of radius r_1, yielding the energy, E_1. Each subsequent point kernel entry, E_i/V_i, is multiplied by the volume V_i of the spherical shell of thickness $r_{i+1}-r_i$, yielding the energy E_i, until the distance r_i equals (interpolating, if necessary) one-half of the diagonal calculated in Step 1. The resulting energies, E_i, are summed to yield the total energy deposited in a sphere of radius equal to one-half of the diagonal calculated in Step 1.
3. Multiply the energy obtained in Step 2 by the cumulated activity concentration in the source volume.
4. Assign this mean local dose to every target point inside the source volume.
5. Apply the algorithm described above (Cf. Eq. 1) only when the distance between a given target-source point pair is greater than one-half the diagonal calculated in Step 1.

Steps 1 through 4 define the mean local dose. The mean local dose is essentially an averaging over the inter-source point distances, it is calculated by multiplying the cumulated activity concentration by the total energy per disintegration that is deposited in a sphere of a given dimension. This approach is similar to that described by the MIRD Committee for calculating the dose due to "non-penetrating" emissions (e.g., electrons) (*2*). The total energy per disintegration corresponds to a sum of the MIRD equilibrium dose constants over these emissions. Our implementation is a modification of the MIRD approach in that the energy per disintegration is determined for a sphere such that the energy deposited outside the sphere is not included in the mean local dose; this energy is accounted for by Equation 1. For nonpenetrating radiations, the MIRD approach assigns all of the emission energy to the emitter point of origin (i.e., electron range is neglected). By using the point source kernel and determining the energy deposited in a given sphere, our technique ignores the electron dose distribution only for electron ranges less than the sphere radius. One should note that if the electron ranges are all shorter than the radius of the sphere, our approach for calculating the mean local dose is equivalent to the MIRD approach. This dose is introduced to eliminate the artifactual variability in inter-source point dose (i.e., for target points within the source volume) caused by representing a continuous distribution of activity by a discrete set of points. An alternative solution, of course, would be to increase the source point density. However, because increasing source point density may dramatically increase computation time with only minimal improvement in accuracy, the source point density should be chosen to satisfy the required spatial resolution, or scale, of the particular treatment plan as dictated by the dimensions of the source volumes (as visualized by external imaging) rather than by the need to eliminate a calculational artifact. In Step 5, the dose contributions to a target point from source points separated by a target-to-source point distance less than or equal to one-half the diagonal calculated in Step 1 (inter-source point spacing) are set to zero since these dose contributions have already been taken into account by the mean local dose (Steps 1 through 4). The dose contributions from source points separated by a target-to-source point distance greater than one-half the diagonal are calculated without modification according to the previously described algorithm (Cf. Eq. 1).

Isodose Contour Display

The final output of the dose calculation portion of IDTP is a two-dimensional matrix of dose values corresponding to the target region grid points specified by the user. The isodose contour display portion of IDTP allows one to superimpose isodose contours on the CT image corresponding to the target plane (*20*, *25*). The program provides a set of eight equally spaced isodose levels, displayed as closed color-coded curves, ranging from zero to the maximum calculated dose in the image. The user may, with a trackball, scan through and view the contour corresponding to any of the dose values achieved. Each contour is color-coded with the corresponding dose. The isodose contour for one or more selected dose values may be displayed, thereby allowing the user to generate a map of the dose distribution over the tissues of interest (see Figures 4, 5, and 6).

RESULTS

The calculational scheme we have described consists of a series of well-defined mathematical steps; no Monte Carlo calculations are performed during a dose calculation. The accuracy of the dose calculation depends upon the accuracy of the point kernel employed and on the accuracy of the calculational approach. EGS has been extensively tested against both experimental measurements and other Monte Carlo stimulation packages (*21*, *22*). The basic algorithm and its implementation have been tested against analytically derived dose estimates using analytically generated point kernels and spherical geometries. Doses resulting from very short-range emitters have been compared with estimates obtained directly from MIRD equilibrium dose constants (dose inside the source volume = equilibrium dose constant × cumulated activity concentration) and are in good agreement (difference < 1%). Doses arising from photon emitters have also been compared (differences < 3%) with MIRD estimates (*26*) for a range of photon energies (0.03-1.50 MeV). The errors associated with neglecting differences in tissue composition and in the interface between tissues will vary depending on the radionuclide emission spectrum.

The results of a treatment plan designed to illustrate IDTP's features are presented in Figures 4–6. Figure 4 depicts the isodose contours due to three small activity-containing tumors within liver. Each tumor was assigned a cumulated activity concentration of 7.4×10^5 MBq-s/ml of iodine-131 (^{131}I) (i.e., an initial activity concentration of 20 μCi/ml and no biologic clearance);

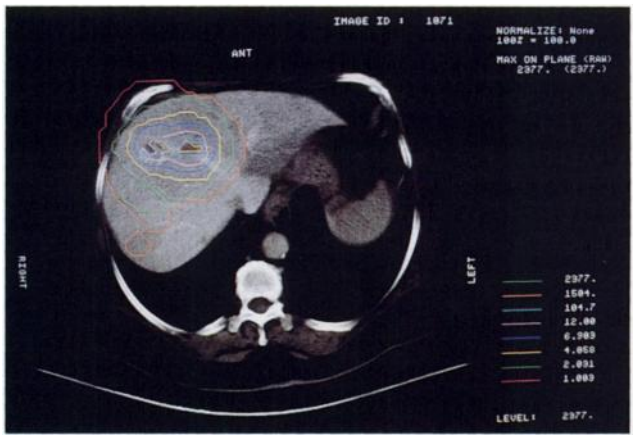

FIGURE 4
A CT image through the liver showing two small tumors in the anterior portion of the liver. The isodose contours resulting from a cumulated activity concentration of 7.4×10^5 MBq-s/ml of ^{131}I in the two visible tumors as well as in a third tumor (not visible in this plane—Cf. Figures 1 and 2) have been overlaid. The dose values (in cGy) assigned to each isodose contour are shown on the lower right. The orange contour is broken into two closed circles both corresponding to a dose of ~1 cGy. The smaller circle is located above the third tumor in the posterior part of the liver and reflects an enhancement in dose due to activity in the third tumor.

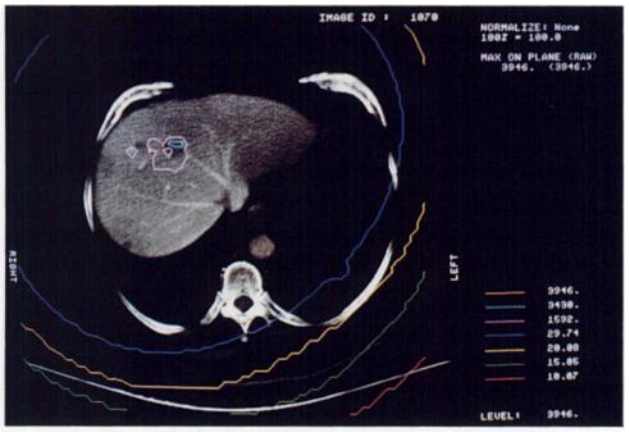

FIGURE 5
A CT image showing the isodose contours resulting from an ^{131}I cumulated activity concentration of 1.1×10^6 MBq-s/ml in each of the three tumors and 3.7×10^5 MBq-s/ml in the normal liver.

a cumulated activity concentration of zero was assigned to the normal liver. In this contrast CT image, two of the tumors are visible as small hypodense regions in the anterior section of the liver. The third tumor is inferior to the level of this CT image and is therefore not visible. Note the rapid decrease in dose outside the tumor regions (i.e., bright orange contour at 1504 cGy to the light blue contour at 105 cGy). The effect on the dose profile from activity in the third tumor is visible at the posterior section of the liver, illustrating the three-dimensional nature of the absorbed dose calculation. Figure 5 depicts isodose contours due to ^{131}I when the normal liver activity concentration is added to that of the three tumors. In this figure, each tumor was assigned a cumulated activity concentration of 1.1×10^6 MBq-s/ml and the normal liver was assigned a cumulated activity concentration of 3.7×10^5 MBq-s/ml. The dose near the surface of the body is ~15 cGy. Figure 6 depicts the isodose contours resulting from the three tumors with an indium-111 (^{111}In) cumulated activity concentration of 2.6×10^6 MBq-s/ml (i.e., an initial activity concentration of 200 μCi/ml and no biologic clearance); no activity has been assigned to normal liver. Note that as a result of the lower energy (0.172, 0.274 MeV) of the ^{111}In photons the radial decrease in dose is much slower than that for ^{131}I (0.364 MeV) (see Fig. 4).

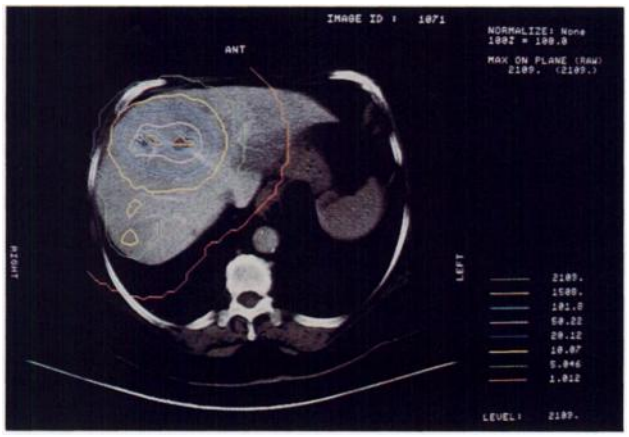

FIGURE 6
The CT image of Figure 4 is shown with the isodose contours resulting from an ^{111}In cumulated activity concentration of 2.6×10^6 in each of the three previously described tumors.

DISCUSSION

We have developed a calculational approach that allows one to obtain position-dependent tissue radiation absorbed dose estimates from irregular and nonuniform distributions of internal radionuclides. The source volumes are defined from patient CT images, thereby allowing for dosimetry calculations based on each individual patient's geometry rather than on "Standard Man" geometry (*1*). Doses are displayed as isodose contours superimposed on a CT image. This allows one to correlate the regional, spatially varying dose with the true patient geometry. Independently determined cumulated activities (*2*, *27*, *28*) must be provided as input data. Methods have been developed for determination of source region activity and/or activity concentration based upon quantitative planar (*29*) and SPECT (*24*) imaging. Recently developed computer algorithms for anatomically matching SPECT three-dimensional activity distributions to CT and MRI scans may facilitate assignment of cumulated activities to anatomical regions as visualized on CT and MRI images (*30–32*).

In interpreting the isodose contours shown in Figures 4–6, one must keep in mind that a key assumption of the algorithm is that of a homogeneous medium, that is, differences in tissue mass and electron mass density are not taken into account. The homogeneous medium assumption is used for photons in external beam treatment planning applications in cases where the beam does not traverse bone or lung (*6*, *20*). When changes in mass or electron density are significant, however, the equivalent path length approach provides a feasible solution (*33*). Although not yet implemented in IDTP, this approach involves scaling the distance between each source and target point according to the composition of the regions traversed. Since the equivalent path length will differ depending on the emission type (e.g., photon, electron, alpha particle) one must resolve the point-kernel into distinct point-kernels corresponding to the respective type of emission. The dose to a target point can then be obtained by calculating the equivalent path length for each type of emission and summing the corresponding doses from each emissions type-specific point-kernel.

The clinical applicability of IDTP in large part will be determined by the time required to generate radiation dose estimates for a particular patient. The majority of time is spent identifying and drawing the contours

for each source volume. The operator first examines each transverse CT image, identifies the subset of images that contain the structure or structures of interest, and then draws the appropriate contour for each structure on each CT slice. The time required to complete this process may take up to several hours depending on the complexity of the particular patient geometry. Most of this time is devoted to human decision making. This time may be minimized by resorting to MIRD calculations whenever possible. In general, MIRD estimates are adequate for calculating the dose to normal tissues that are not in close proximity to the tumor tissue. By limiting IDTP calculations to determinations of tumor and adjacent tissue dose [cases which are not amenable to the MIRD "Standard Man" formalism (*1*)], one may significantly reduce the number of contours required and thereby the operator time. The illustrative calculations depicted in Figures 4–6 as well as the time estimates for completing the computer intensive tasks listed below were obtained using a Digital Equipment Corporation VAX 8550 computer (without an array processor) under normal operating conditions (i.e., an average of 5 to 10 users logged on simultaneously). The computer-intensive tasks are the following:

1. Reading images from the CT magnetic tape, translating the various CT scanner formats to a common format, and copying them to the hard disk. This typically takes 25 sec per image or 10 to 20 min per patient study. Once the transfer is initiated, however, no further user input is required.
2. Performing the dose calculation. The time required for this increases linearly with the source volume and target plane dimensions and in inverse proportion to the cube of the source and to the square of the target grid spacing. Each of the calculations depicted in Figures 4 and 6 in which activity was assigned to each of the three basic hepatic tumor took ~30 sec. The calculation depicted in Figure 5 in which the activity was assigned to the whole liver as well as to the three hepatic tumors took more than 2 hr and was obtained by an overnight batch mode execution.

Both computer-intensive tasks require minimal user interaction and are therefore not limiting in terms of personnel time. The time required to complete these tasks will drop significantly as IDTP is modified to take advantage of currently existing specialized hardware (e.g., array processors, dedicated work stations). The user-intensive portion of the program, however, (i.e., the source volume identification) is not subject to the same potential improvements since it is dependent on human decision making rather than on the speed of the hardware. Developments in artificial intelligence might some day reduce the time required for this task by aiding or reducing the user-dependent decision making process.

In light of the increased interest in dose distributions at the cellular level (*34–36*), it should be noted that the approach we have presented for macroscopic dosimetry may be adapted to cell-level dosimetry calculations. By a scale transformation (i.e., input of a point kernel that describes dose deposition over microns rather than centimeters) and using autoradiographic images of radionuclide distributions within a cell or cell cluster rather than patient CT images one may (in an identical calculational manner) obtain dose distributions across cellular dimensions. Such calculations will be especially valuable in assessing the "dose enhancement" resulting from nonuniform depositions of very short-range emitters at the cellular level.

ACKNOWLEDGMENTS

This work was supported by NCI Contract N01-CM37565 and NCI Grant P01CA-29502. Presented at the Annual Meeting of The Society of Nuclear Medicine, June 1988, San Francisco, California.

REFERENCES

1. International Commission on Radiological Protection. Report of the task group on reference man. *ICRP Publication 23*. New York: Pergamon Press; 1975.
2. Loevinger R, Berman M. A revised schema for calculating the absorbed dose from biologically distributed radionuclides. *MIRD Pamphlet No. 1, Revised.* New York: Society of Nuclear Medicine; 1976.
3. Snyder WS, Ford MR, Warner GG. Estimates of specific absorbed fractions for photon sources uniformly distributed in various organs of a heterogeneous phantom. *MIRD Pamphlet No. 5, Revised.* New York: Society of Nuclear Medicine; 1978.
4. Snyder WS, Ford MR, Warner GG, Watson SB: "S," absorbed dose per unit cumulated activity for selected radionuclides and organs. *MIRD Pamphlet No. 11, Revised.* New York: Society of Nuclear Medicine; 1975.
5. Sgouros G, Barest G, Thekkumthala J, et al. Treatment planning for monoclonal antibody therapy: three-dimensional dosimetry for nonuniformly distributed radionuclides [Abstract]. *J Nucl Med* 1988; 29:803.
6. Mohan R, Barest G, Brewster LJ, et al. A comprehensive three-dimensional treatment planning system. *Int J Radiat Oncol Biol Phys* 1988; 15:481–495.
7. Fraas BA, McShan DL, Weeks KL. 3-D treatment planning: III. Complete beam's-eye-view planning capabilities. In: Bruinvis IAD, van der Giessen PH, van Kleffens HJ, Wittkamper FW, eds. *Ninth international conference on the use of computers in radiation therapy.* The Hague, Netherlands; 1987:193–195.
8. Goitein M, Abrams M, Rowell D, Pollari H, Wiles J. Multidimensional treatment planning: II. Beam's-eye-view, back projection through CT sections. *Int J Radiat Oncol Biol Phys* 1983; 9:789–797.
9. International Commission on Radiological Protection.

Radionuclide transformations: energy and intensity of emissions. ICRP Publication 38, New York: Pergamon Press; 1983.
10. Berger MJ. Energy deposition in water by photons from point isotropic sources. MIRD pamphlet no. 2. *J Nucl Med* 1968; 1:15–25.
11. Berger MJ. Distribution of absorbed dose around point sources of electrons and beta particles in water and other media. *J Nucl Med* 1971; 12(Suppl 5):7–23.
12. Berger MJ. Improved point kernels for electron and beta-ray dosimetry. Progress Report No. NBSIR 73-107, Center for Radiation Research, National Bureau of Standards. Washington, DC; 1973.
13. Cross WG, Ing H, Freedman NO, Mainville J. Tables of beta-ray dose distribution in water, air and other media. Report No. AECL-7617, Atomic Energy of Canada Limited, Chalk River, Ontario; 1982.
14. Prestwich WV, Chan LB, Kwok CS, Wilson B. Dose point kernels for beta-emitting radioisotopes. In: *Proceedings of the fourth international radiopharmaceutical dosimetry symposium.* Oak Ridge, TN: US Department of Energy Publ No DE 86010102; 1985:545–561.
15. Bigler RE (Principal Investigator). *Dose calculations for cancer therapy using radioactively labeled antibodies directed to tumor-associated and/or tumor-specific antigens,* 1st-5th Semi-Annual Reports. National Cancer Institute Contract N01-CM-37565; 1984–1986.
16. Polig E. The localized dosimetry of internally deposited alpha-emitters. *Curr Top Rad Res* 1978; 13:189–327.
17. Cole A. Absorption of 20-eV to 50,000-eV electron beams in air and plastic. *Radiat Res* 1969; 38:7–33.
18. Ford RL, Nelson WR. The EGS code system. *Stanford linear accelerator center report.* No. 210, Stanford, California; 1978.
19. Dillman LT, EDISTR-A computer program to obtain a nuclear decay data base for radiation dosimetry, ORNL/TM-6689, Radiation Shielding Information Center, Oak Ridge National Laboratory, Oak Ridge, TN; 1980.
20. Mohan R, Antich PP. A method of correction for curvature and inhomogeneities in computer aided calculation of external beam radiation dose distributions. *Comput Prog Biomed* 1979; 9:247–257.
21. Rogers DWO, Bielajew AF. A Comparison of EGS and ETRAN. In: Jenkins TM, Nelson WR, Rindi A, eds. *Monte Carlo transport of electrons and photons.* New York: Plenum Press; 1988.
22. Rogers DWO, Bielajew AF. Experimental benchmarks of EGS. In: Jenkins TM, Nelson WR, Rindi A, eds. *Monte Carlo transport of electrons and photons.* New York: Plenum Press; 1988.
23. Berger MJ, Seltzer SM, ETRAN, Monte Carlo code system for electron and photon transport through extended media. ORNL Documentation for RSIC Computer Code Package CCC-107; 1973.
24. Zanzonico PB, Bigler RE, Sgouros G, Strauss A. Quantitative SPECT in radiation dosimetry. *Semin Nucl Med* 1989; 19:47–61.
25. Brewster L, Mohan R, Barest G. Dose distribution display techniques in radition therapy. *National computer graphics association computer graphics '87 conference proceedings.* Fairfax, VA, NCGA; 1987.
26. Ellett WH, Humes RM. Absorbed fractions for small volumes containing photon-emitting radioactivity. *MIRD pamphlet no. 8.* New York: Society of Nuclear Medicine; 1971.
27. Zanzonico PB, Bigler RE, Primus FJ, et al. A compartmental modeling approach to the radiation dosimetry of radiolabeled antibody. In: Schlafke-Stelson AT, Watson EE, eds. *Proceedings of the fourth international radiopharmaceutical dosimetry symposium.* Oak Ridge, TN, CONF-851113-DE86010102; 1985:421–445.
28. Koral KF, Wang X, Sisson JC, et al. Calculating radiation absorbed dose for phoechromocytoma tumors in 131-I MIBG therapy. *Int J Radiat Oncol Biol Phys* 1989; 17:211–218.
29. Zanzonico PB, Sgouros G, Strauss A, Bigler RE. Treatment planning for monoclonal antibody therapy: quantitative planar imaging and its validation using an anthropomorphic phantom [Abstract]. *J Nucl Med* 1988; 29:845.
30. Chen GTY and Pelizzari CA, Image Analysis and Processing in Radiation Therapy Planning. In: Brady LJ, Hall EJ, Sheline GE, Smith AR, eds. Radiation Oncology Research Directions. *Am J Clin Oncol* 1988; 11(3):190–194.
31. Levin DN, Pelizzari CA, Chen GTY, Chen C, Cooper MD. Retrospective geometric correlation of MR, CT, and PET images. *Radiology* 1988; 169:817–823.
32. Kramer EL, Noz ME, Sanger JJ, Megibow AJ, Maguire GQ. CT-SPECT fusion to correlate radiolabeled monoclonal antibody uptake with abdominal CT findings. *Radiology* 1989; 172:861–865.
33. Mohan R, Chui C, Miller D, Laughlin JS. Use of computerized tomography in dose calculations for radiation treatment planning. *J Comp Tomog* 1981; 5:273–282.
34. Bigler RE, Zanzonico PB, Cosma M, Sgouros G. Adjuvant radioimmunotherapy for micrometastases: a strategy for cancer cure: In: Srivastava SC, ed. *Radiolabeled monoclonal antibodies for imaging and therapy.* New York: Plenum Press; 1988:409–429.
35. Makrigiorgos GM, Adelstein SJ, Kasis AI. Limitations of conventional internal dosimetry at the cellular level. *J Nucl Med* 1989; 30:1856–1864.
36. Humm JL, Cobb LM. Nonuniformity of tumor dose in radioimmunotherapy. *J Nucl Med* 1990; 31:75–83.